Strangeness-correlations on the pseudocritical line in (2 + 1)-flavor QCD

D. Bollweg,[1] H.-T. Ding,[2] J. Goswami,[3] F. Karsch,[4] Swagato Mukherjee,[5]
P. Petreczky,[5] and C. Schmidt[4]

[1]*Computational Science Initiative, Brookhaven National Laboratory, Upton, New York 11973, USA*
[2]*Key Laboratory of Quark & Lepton Physics (MOE) and Institute of Particle Physics,
Central China Normal University, Wuhan 430079, China*
[3]*RIKEN Center for Computational Science, Kobe 650-0047, Japan*
[4]*Fakultät für Physik, Universität Bielefeld, D-33615 Bielefeld, Germany*
[5]*Physics Department, Brookhaven National Laboratory, Upton, New York 11973, USA*

We present some lattice QCD results on first (χ_1^i) and second (χ_2^i) cumulants of and correlations (χ_{11}^{ij}) among net baryon-number (B), strangeness (S) and electric charge (Q) along the pseudocritical line [$T_{pc}(\mu_B)$] in the temperature (T)–baryon chemical potential (μ_B) phase diagram of (2 + 1)-flavor QCD. We point out that violations of sum rules among second order cumulants, which hold in the isospin symmetric limit of vanishing electric charge chemical potential, are small along the $T_{pc}(\mu_B)$ for the entire range of μ_B covered in the RHIC beam energy scan. For the strangeness neutral matter produced in heavy-ion collisions this leads to a close relation between χ_{11}^{BS} and χ_{11}^{QS}. We compare lattice QCD results for χ_{11}^{BS}/χ_2^S along the $T_{pc}(\mu_B)$ line with preliminary experimental measurements of χ_{11}^{BS}/χ_2^S for collision energies 7.7 GeV $\leq \sqrt{s_{NN}} \leq$ 62.4 GeV. While we find good agreements for $\sqrt{s_{NN}} \geq$ 39 GeV, differences are sizeable at smaller values of $\sqrt{s_{NN}}$. Moreover, we compare lattice QCD results for the ratio of the strangeness (μ_S) to baryon (μ_B) chemical potentials, which define a strangeness neutral system with fixed electric charge to baryon number density, with experimental results obtained by the STAR collaboration for μ_S/μ_B using strange baryon yields on the freeze-out line. Finally, we determine the baryon chemical potential at the freeze-out (μ_B^f) by comparing χ_1^B/χ_2^B along the $T_{pc}(\mu_B)$ with the experimentally measured net-proton cumulants χ_1^p/χ_2^p. We find that $\{\mu_B^f, T_{pc}(\mu_B^f)\}$ are consistent with the freeze-out parameters of the statistical-model fits to experimentally measured hadron yields for $\sqrt{s_{NN}} \geq$ 11.5 GeV.

I. INTRODUCTION

Higher order cumulants of fluctuations of conserved charges and correlations among different conserved charges of quantum chromodynamics (QCD) are sensitive observables for the occurrence of phase transitions in strongly interacting matter and reflect the change of relevant degrees of freedom responsible for fluctuations and correlations in hot and dense strong-interaction matter. In particular, correlations between conserved, net baryon number and net strangeness number have been suggested as sensitive probes [1] for the change of degrees of freedom carrying strangeness at low temperature (hadrons) and high temperature (quarks), respectively. The temperature and density

dependence of conserved charge fluctuations and their higher order cumulants is studied in lattice QCD calculations using Taylor series expansions as well as in numerical simulations with imaginary chemical potentials [2–5].

Experimentally the cumulants of conserved charge densities are not directly accessible. E.g. net proton [6] or kaon number [7–9] fluctuations and correlations among them are used as proxies for baryon or strangeness number fluctuations. Incorporating strange baryon contributions also allows to construct proxies for strangeness and baryon number as well as strangeness and electric charge correlations [9–11].

The experimentally observed charge fluctuations and correlations are expected to be generated at the so-called chemical freeze-out temperature T_f. Also this temperature and the baryon as well as strangeness chemical potentials (μ_B^f, μ_S^f) that control the thermal conditions at the time of freeze-out are not directly accessible in heavy ion collisions. Eventually they could be deduced through a comparison of experimental data with QCD thermodynamics,

if the medium is in equilibrium at the time of freeze-out. In practice the experimental determination of freeze-out parameters involves a model dependent step. Experimentally determined particle yields are compared to hadronization models [12–14]. The thus determined freeze-out temperature at various values of the beam energy, $T_f(\sqrt{s_{NN}})$, is found to be in good agreement with the pseudocritical temperature, $T_{pc}(\hat{\mu}_B)$, that is determined in lattice QCD calculations [15,16]. Generally this is taken as support for the assumption that hadron resonance gas (HRG) models provide a good approximation to the thermodynamics of strong-interaction matter at the time of freeze-out.

Aside from studies of higher order cumulants of proxies for net baryon-number fluctuations, the calculation of correlations between low order cumulants of conserved charge densities, e.g. correlation of net strangeness and net baryon-number, is being performed in the beam energy scan at RHIC. We previously presented comparisons of higher order cumulants of net baryon-number fluctuations with results obtained by the STAR collaboration [17,18] for the related proton number cumulants. We also compared results of the STAR collaboration on strange hadron yields at several values of the beam energy [9] with lattice QCD results [19,20] on correlations between net baryon-number and strangeness. This provided evidence for the influence of additional strange hadrons, not listed by the Particle Data Group as established strange hadron resonances [21].

We previously also calculated low order cumulants of net baryon-number fluctuations at nonzero values of the baryon chemical potential, using high statistics datasets generated in $(2 + 1)$-flavor QCD calculations at finite temperature [22,23]. In these calculations we focused on an analysis of second order cumulants at vanishing values of the chemical potentials as well as an analysis of the convergence of the Taylor series and the comparison with Padé resummed results obtained from such series expansions. We concluded that expansions of second order cumulants, in particular the second order cumulant for net baryon-number fluctuations, are well controlled for baryon chemical potentials $\mu_B/T \lesssim 1.5$.

We extend this analysis here by calculating correlations between conserved charge densities as function of the baryon chemical potential on the pseudocritical line in $(2 + 1)$-flavor QCD using Taylor series for second order cumulants up to NNLO order, i.e., up to $\mathcal{O}(\mu_B^4)$. We will use these results to compare with recent preliminary results of the STAR collaboration obtained for correlations between net baryon number and strangeness densities [24].

The data sets used for our calculation and further details relevant for our data analysis, have been described previously in Sec. II of [17] and the number of configurations, used for our current work, are given in Table I of [17]. In particular, as discussed in [17], using fits of lattice QCD results obtained at different values of the lattice spacing to rational polynomials, we obtain continuum extrapolated

estimates for the $\hat{\mu}_B$-dependence of various second order cumulants on the pseudocritical line, $T_{pc}(\hat{\mu}_B)$, as well as extrapolations performed directly for ratios of second order cumulants.

This paper is organized as follows. In Sec. II we introduce basic formulasd used for the calculation of Taylor expansions of second order cumulants. In Sec. III we present results for various second order cumulants obtained in lattice QCD calculations as functions of T and $\hat{\mu}_B$. In Sec. IV we present results for these cumulants evaluated on the pseudocritical line $T_{pc}(\mu_B)$ and compare them with recent results of the STAR collaboration obtained during the beam energy runs BES-II at RHIC. We give our conclusions in Sec. V. In an Appendix we give some explicit expressions for the expansion of second order cumulants up to $\mathcal{O}(\mu_B^4)$.

II. CUMULANTS OF CONSERVED CHARGE DENSITIES

Cumulants of conserved charge fluctuations at vanishing chemical potentials for the conserved charges of $(2 + 1)$-flavor QCD, *i.e.* net baryon-number (B), electric charge (Q) and strangeness (S), are obtained from the QCD partition function, $\mathcal{Z}(T, V, \vec{\mu})$, as derivatives with respect to the associated chemical potentials $\vec{\mu} = (\mu_B, \mu_Q, \mu_S)$,

$$\chi_{ijk}^{BQS}(T, V) = \frac{1}{VT^3} \frac{\partial \ln \mathcal{Z}(T, V, \vec{\mu})}{\partial \hat{\mu}_B^i \partial \hat{\mu}_Q^j \partial \hat{\mu}_S^k}\bigg|_{\vec{\mu}=0}, \quad (1)$$

with $\hat{\mu}_X \equiv \mu_X/T$. These cumulants can be used to set up Taylor series for cumulants at nonzero values of the chemical potentials. Starting with the Taylor series for the pressure,

$$\frac{P}{T^4} = \frac{1}{VT^3} \ln \mathcal{Z}(T, V, \vec{\mu}) = \sum_{i,j,k=0}^{\infty} \frac{\chi_{ijk}^{BQS}}{i!j!k!} \hat{\mu}_B^i \hat{\mu}_Q^j \hat{\mu}_S^k, \quad (2)$$

we easily obtain series for second order cumulants by taking appropriate derivatives with respect to the chemical potentials. In these Taylor series we replace the chemical potentials $\hat{\mu}_Q$ and $\hat{\mu}_S$ by series in terms of $\hat{\mu}_B$ only,

$$\mu_S/\mu_B = \sum_{i=0}^{\infty} s_{2i+1}(T) \hat{\mu}_B^{2i+1}, \quad (3)$$

$$\mu_Q/\mu_B = \sum_{i=0}^{\infty} q_{2i+1}(T) \hat{\mu}_B^{2i+1}, \quad (4)$$

where the coefficients s_i, q_i are fixed through constraints on the net baryon-number density,[1] n_B, and the ratio of electric

---

[1]We use here and in the following dimensionless number densities. I.e. densities n_X, $X = B, Q, S$, are given in units of T^3.

charge and strangeness densities, n_Q/n_S. We demand strangeness neutrality, $n_S = 0$, and a fixed ratio of net electric charge and baryon number densities, $n_Q/n_B = 0.4$, which is consistent with experimental conditions realized in heavy ion collisions of lead-lead or gold-gold nuclei. The resultant coefficients s_i, q_i are given in [25] for $i = 1, 3, 5$. With this we obtain for the next-to-leading order (NLO) expansion of second order cumulants

$$\chi_{11}^{BS}(T,\vec{\mu}) = \chi_{11}^{BS} + \frac{\hat{\mu}_B^2}{2!}[\chi_{31}^{BS} + 2s_1\chi_{22}^{BS} + s_1^2\chi_{13}^{BS} + 2q_1\chi_{211}^{BQS}$$
$$+ 2q_1s_1\chi_{112}^{BQS} + q_1^2\chi_{121}^{BQS}] + \mathcal{O}(\hat{\mu}_B^4), \tag{5}$$

$$\chi_{11}^{QS}(T,\vec{\mu}) = \chi_{11}^{QS} + \frac{\hat{\mu}_B^2}{2!}[\chi_{211}^{BQS} + 2s_1\chi_{112}^{BQS} + s_1^2\chi_{13}^{QS} + 2q_1\chi_{121}^{BQS}$$
$$+ 2q_1s_1\chi_{22}^{QS} + q_1^2\chi_{31}^{QS}] + \mathcal{O}(\hat{\mu}_B^4), \tag{6}$$

$$\chi_2^S(T,\vec{\mu}) = \chi_2^S + \frac{\hat{\mu}_B^2}{2!}[\chi_{22}^{BS} + s_1^2\chi_4^S + 2s_1\chi_{13}^{BS}$$
$$+ 2q_1\chi_{112}^{BQS} + 2q_1s_1\chi_{13}^{QS} + q_1^2\chi_{22}^{QS}] + \mathcal{O}(\hat{\mu}_B^4), \tag{7}$$

$$\chi_2^B(T,\vec{\mu}) = \chi_2^B + \frac{\hat{\mu}_B^2}{2!}[\chi_4^B + s_1^2\chi_{22}^{BS} + 2s_1\chi_{31}^{BS} + 2q_1\chi_{31}^{BQ}$$
$$+ 2q_1s_1\chi_{211}^{BQS} + q_1^2\chi_{22}^{BQ}] + \mathcal{O}(\hat{\mu}_B^4). \tag{8}$$

Explicit expressions for the order $\mathcal{O}(\hat{\mu}_B^4)$ (NNLO) expansion coefficients, which we will use in the following, are given in Appendix.

The leading order μ_S/μ_B is related with the χ_{11}^{BS}/χ_2^S in the following way,

$$\frac{\mu_S}{\mu_B} = -\frac{\chi_{11}^{BS}(T,0)}{\chi_2^S(T,0)} - \frac{\chi_{11}^{QS}(T,0)}{\chi_2^S(T,0)}q_1 + \mathcal{O}(\mu_B^2). \tag{9}$$

In the case of degenerate up and down quark masses, which generally is used in lattice QCD calculations, the cumulants χ_{11}^{BS}, χ_{11}^{QS}, and χ_2^S are directly related to each other,

$$2\frac{\chi_{11}^{QS}(T,\vec{\mu})}{\chi_2^S(T,\vec{\mu})} - \frac{\chi_{11}^{BS}(T,\vec{\mu})}{\chi_2^S(T,\vec{\mu})} = 1 + \frac{\Delta^{BQS}(T,\vec{\mu})}{\chi_2^S(T,\vec{\mu})}. \tag{10}$$

For $\mu_Q \neq 0$, one finds,

$$\Delta^{BQS}(T,\vec{\mu}) = q_1\frac{\hat{\mu}_B^2}{2}(q_1(2\chi_{031}^{BQS} - \chi_{022}^{BQS} - \chi_{121}^{BQS})$$
$$- s_1(2\chi_{013}^{BQS} - 4\chi_{022}^{BQS} + 2\chi_{112}^{BQS})$$
$$- \chi_{103}^{BQS} + 4\chi_{121}^{BQS} - 2\chi_{202}^{BQS} - \chi_{301}^{BQS})$$
$$+ \mathcal{O}(\hat{\mu}_B^4). \tag{11}$$

At vanishing electric charge chemical potential μ_Q, i.e., in the isospin symmetric case with $n_Q/n_B = 0.5$, one thus obtains the sum rule,

$$\Delta^{BQS}(T,\vec{\mu}) = 0, \quad \text{for } \vec{\mu} = (\mu_B, 0, \mu_S). \tag{12}$$

We will compare results for the second order cumulants with HRG model calculations based on the list of hadrons published in the tables of the Particle Data group [21] (PDG-HRG) as well as the QMHRG2020 list compiled by the HotQCD Collaboration [23,26]. In order to probe the validity of Eq. (12) and the isospin symmetry violations induced by a nonvanishing electric charge chemical potential in HRG model calculations, we introduced an isospin symmetric version of these hadron lists. For this purpose we set masses for charged strange hadrons equal to the masses of their neutral partners. This concerns 7 strange hadrons, for which mass differences are listed in the PDG tables: $K, K^*, K_2^*, \Sigma, \Sigma(1385), \Xi, \Xi(1530)$. In all these cases isospin violations, arising from the mass differences between charged and neutral strange hadrons, are below 1%. We note that setting the masses equal leads only to small changes in the Boltzmann weights entering HRG model calculations. In the vicinity of the pseudocritical temperature $T_{pc,0} = 156.5(1.5)$ MeV [15] this amounts to about 0.6%. In general this small difference is negligible. However, when comparing QCD and HRG model results for Δ^{BQS} as given in Eq. (11), this small change leads to differences which are of the same magnitude as the modifications induced by a nonvanishing electric charge chemical potential itself.

III. SECOND ORDER CUMULANTS AS A FUNCTION OF TEMPERATURE AND BARYON CHEMICAL POTENTIAL

In [23] we presented continuum extrapolated results for all second order cumulants at vanishing values of the chemical potentials. For nonvanishing values of the chemical potentials Taylor series for the diagonal second order net baryon-number cumulant, $\chi_2^B(T,\hat{\mu}_B)$, have been presented in [17]. Some preliminary results on strangeness correlations and fluctuations at nonzero $\hat{\mu}_B$ have also been shown in [20,27].

Here we focus on the behavior of off-diagonal, second order cumulants. We concentrate on a discussion of correlations between net strangeness number (n_S) and net baryon-number (n_B) densities as well as n_S and net electric charge (n_Q) density. We shall consider thermal conditions that are of relevance for comparisons with experimental conditions realized in heavy ion collisions, i.e. we consider a thermal medium with vanishing net strangeness, $n_S = 0$, and $n_Q/n_B = 0.4$.

In Fig. 1 we show the ratios $-\chi_{11}^{BS}(T,\hat{\mu}_B)/\chi_2^S(T,\hat{\mu}_B)$ (top) and $\chi_{11}^{QS}(T,\hat{\mu}_B)/\chi_2^S(T,\hat{\mu}_B)$ (bottom), obtained from $\mathcal{O}(\hat{\mu}_B^2)$
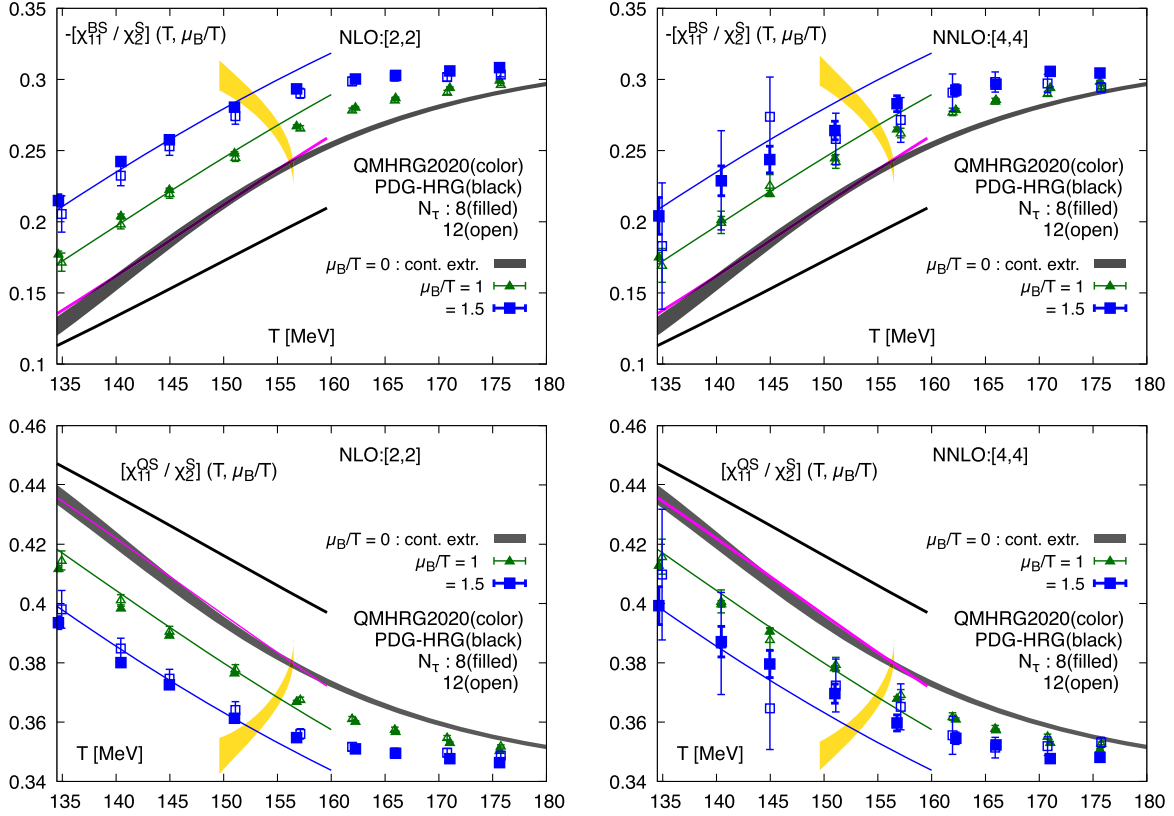
FIG. 1.   Top: correlation between net baryon-number and strangeness number densities normalized to the second order cumulant of strangeness fluctuations versus T for several values of $\hat{\mu}_B$. Shown are results obtained on lattices with temporal extent $N_\tau = 8$ (filled symbols) and 12 (open symbols) from $\mathcal{O}(\hat{\mu}_B^2)$ (left) and $\mathcal{O}(\hat{\mu}_B^4)$ (right) Taylor series for χ_{11}^{BS} and χ_2^S, respectively. The lattice QCD results are compared to HRG model calculations using the QMHRG2020 list (colored lines). For $\hat{\mu}_B = 0$ also a result based on the PDG-HRG list is shown (black line). The gray band shows the continuum extrapolated results (cont. extr.) for the second order cumulant ratio at vanishing chemical potential [23]. The yellow band shows the location of the pseudocritical line $T_{pc}(\hat{\mu}_B)$. Bottom: same as figures on the top, but for correlation between net electric charge and strangeness densities normalized to the second order cumulant of strangeness fluctuations.

(left) and $\mathcal{O}(\hat{\mu}_B^4)$ (right) Taylor series, respectively. As can be seen these expansions agree well for small $\hat{\mu}_B$. The second and fourth order expansions start to differ at temperatures below the pseudocritical line for the chiral transition (yellow bands) at $\hat{\mu}_B \simeq 1.5$.

The lattice QCD results are compared to HRG model calculations that utilize the PDG-HRG and QMHRG2020 lists. As noted already in the analysis of second order cumulants at vanishing chemical potential [23] HRG model calculations based on the QMHRG2020 list describe the lattice QCD results well at low temperatures up to $T_{pc}(\hat{\mu}_B)$. HRG model calculations based on the PDG-HRG list [21], however, are insufficient already for $T \gtrsim 130$ MeV. While QMHRG2020 and lattice QCD calculations agree well at $T_{pc,0} \equiv T_{pc}(0)$, differences become larger with increasing $\hat{\mu}_B$ also on the pseudocritical line.

The pseudocritical line has been determined in lattice QCD calculations as a Taylor series up to $\mathcal{O}(\hat{\mu}_B^4)$ [15,16,28],

$$T_{pc}(\mu_B) = T_{pc,0}[1 - \kappa_2 \hat{\mu}_B^2 + \kappa_4 \hat{\mu}_B^4]. \quad (13)$$

We use results from [15], i.e., $T_{pc,0} = (156.5 \pm 1.5)$ MeV and $\kappa_2 = 0.012(4)$. Within errors this is in agreement with results obtained in [16,28]. The $\mathcal{O}(\hat{\mu}_B^4)$ correction in Eq. (13) has been found to vanish within current statistical errors [15,16]. We leave out the contribution of the $O(\hat{\mu}_B^4)$ in the following as it as been found to vanish within current statistical errors [15,16]. I.e. Ref. [15] found $\kappa_4 = 0.000(4)$ and Ref. [16] reported $\kappa_4 = 0.00032(67)$. The pseudocritical temperature $T_{pc}(\hat{\mu}_B)$ is shown in Fig. 1 as a yellow band.

As can be seen in Fig. 1 the magnitude of the ratio $\chi_{11}^{BS}(T, \hat{\mu}_B)/\chi_2^S(T, \hat{\mu}_B)$ increases with increasing $\hat{\mu}_B$. On the pseudocritical line this amounts to only a moderate change of about (15–20)% between $\hat{\mu}_B = 0$ and 1.5.

In the previous section we pointed out that the sum rule, $2\chi_{11}^{QS} - \chi_{11}^{BS} = \chi_2^S$, holds in QCD at any value of the
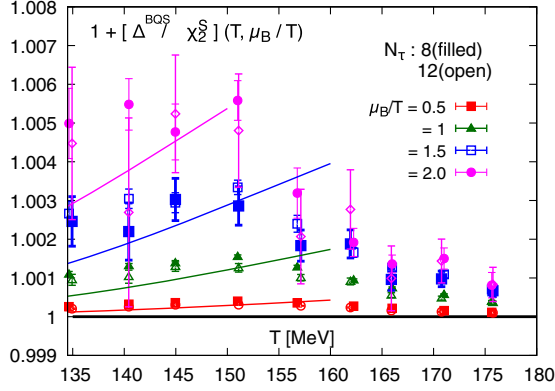
FIG. 2. Deviations from the sum rule, Eq. (14), valid in isospin symmetric matter for the relation between strangeness and baryon-number correlation on the one hand, and strangeness and electric charge correlations on the other hand. Shown are lattice QCD results using 4th order Taylor series results for the second order cumulants. Also shown are HRG model calculations using the QMHRG2020 list with additional isospin symmetrization for 7 strange hadrons as discussed in Sec. II.

temperature for isospin symmetric matter, i.e., for $\mu_Q = 0$. The difference of the cumulant ratios χ_{11}^{BS}/χ_2^S and $2\chi_{11}^{QS}/\chi_2^S$ thus equals unity for all $\hat{\mu}_Q = 0$,

$$2\frac{\chi_{11}^{QS}(T, \vec{\mu})}{\chi_2^S(T, \vec{\mu})} - \frac{\chi_{11}^{BS}(T, \vec{\mu})}{\chi_2^S(T, \vec{\mu})} = 1 \quad \text{for } \vec{\mu} = (\mu_B, 0, \mu_S). \quad (14)$$

For $\hat{\mu}_Q \neq 0$, e.g. for $n_Q/n_B = 0.4$, we find that deviations from unity increase with increasing $\hat{\mu}_B$. Deviations are largest in the vicinity of $T_{pc}(\hat{\mu}_B)$. However, they stay below[2] 0.5% even for $\hat{\mu}_B \simeq 2$. This is evident from the fourth order Taylor series results shown in Fig. 2. At $\hat{\mu}_B = 2$ the pseudocritical temperature is about $T_{pc}(\hat{\mu}_B = 2) \simeq 150$ MeV. The corresponding baryon chemical potential thus is $\mu_B \simeq 300$ MeV, which corresponds to conditions reached in heavy ion collisions at beam energies below 11.5 GeV. We thus expect Eq. (14) to hold for correlations of net baryon number or electric charge with net strangeness number at the LHC and also at RHIC for almost the entire range of beam energies covered in the beam energy scan.

We finally also note that the sum of χ_{11}^{BS} and χ_{11}^{QS} gives the correlation between light and strange quark densities for any value of the chemical potentials $\vec{\mu}$,

$$\chi_{11}^{us}(T, \vec{\mu}) = -\left(\chi_{11}^{BS}(T, \vec{\mu}) + \chi_{11}^{QS}(T, \vec{\mu})\right). \quad (15)$$

___

[2]Note that isospin violations in QCD at nonzero temperature are indeed expected to be negligible [29]. Nonetheless large violations of isospin symmetry have been reported recently to occur in kaon production in high-energy nucleus-nucleus collisions [30,31].
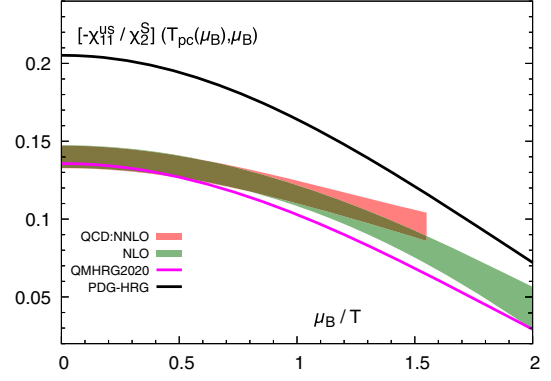

FIG. 3. Correlation between light and strange quark-number densities on the pseudocritical line. Shown are continuum estimates for second and fourth order Taylor expansion results for $-\chi_{11}^{us}/\chi_2^S$ on the pseudocritical line that have been obtained from fits to data obtained in simulations on lattices with temporal extent $N_\tau = 8$ and 12. These results are compared with HRG model results based on the PDG-HRG and QMHRG2020 hadron lists, respectively.

Making use of the very well satisfied sum rule between the second order strange cumulants [cf. Eq. (14)] we thus find that χ_{11}^{BS} also provides a good approximation for the correlation between light and strange quark densities,

$$\frac{\chi_{11}^{us}(T, \hat{\mu}_B)}{\chi_2^S(T, \hat{\mu}_B)} = -\left(\frac{\chi_{11}^{BS}(T, \hat{\mu}_B)}{\chi_2^S(T, \hat{\mu}_B)} + \frac{\chi_{11}^{QS}(T, \hat{\mu}_B)}{\chi_2^S(T, \hat{\mu}_B)}\right) \quad (16)$$

$$\simeq -\frac{1}{2}\left(1 + 3\frac{\chi_{11}^{BS}(T, \hat{\mu}_B)}{\chi_2^S(T, \hat{\mu}_B)}\right). \quad (17)$$

We show QCD results for the correlation between light and strange quark densities on the pseudocritical line in Fig. 3. We note that the magnitude of the light and strange quark correlations decrease with increasing $\hat{\mu}_B$ in HRG model calculations as well as in the QCD calculation. This arises from the increasing importance of multiple strange baryon contributions on the pseudocritical line.

IV. SECOND ORDER CUMULANTS ON THE PSEUDOCRITICAL LINE

A. Pseudocritical line and experimentally determined freeze-out conditions

On the pseudocritical line, $T_{pc}(\hat{\mu}_B)$, the ratio of strangeness and baryon chemical potentials obtained by demanding $n_S = 0$ varies little with increasing $\hat{\mu}_B$. Taylor expansion results for μ_S/μ_B are shown in Fig. 4 and are compared with experimental results obtained by the STAR Collaboration by either fitting particle yields for a large set of strange and nonstrange hadrons to a HRG motivated hadronization model [13] or by fitting only yields of strange baryons [9,13]. Also shown in this figure are values for μ_S/μ_B obtained in HRG model calculations
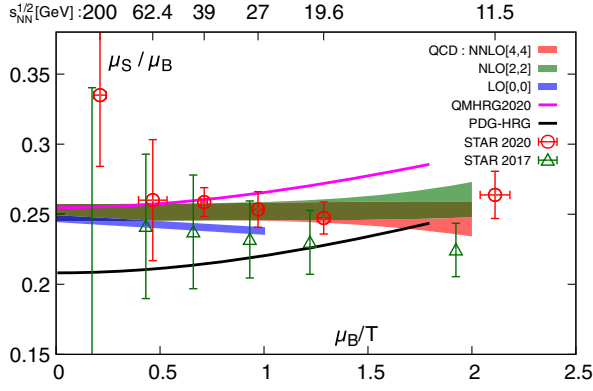
FIG. 4.   The ratio μ_S/μ_B on the pseudocritical line in $(2+1)$-flavor QCD versus $\hat{\mu}_B$ obtained for strangeness neutral matter with $n_Q/n_B = 0.4$. The bands show continuum estimates for second and fourth order Taylor expansion results of μ_S/μ_B on the pseudocritical line that have been obtained from fits to data obtained in simulations on lattices with temporal extent $N_\tau = 8$ and 12. Also shown are results obtained by the STAR Collaboration [9,13,32] and HRG model calculations using the PDG-HRG and QMHRG2020 particle lists, respectively.

based on the PDG-HRG and QMHRG2020 lists for hadron resonances. It is apparent that the former does not describe the QCD results well, whereas the QMHRG2020 provides a good description of μ_S/μ_B on the pseudocritical line at least for $\hat{\mu}_B \lesssim 1$. Beyond this small deviations from the QCD results also show up. HRG model results based on PDG-HRG and QMHRG2020 differ by about 20%. This is similar to the differences found for the ratio χ_{11}^{BS}/χ_2^S. The good agreement between QCD and HRG model calculations based on QMHRG2020 at $T_{pc}(\hat{\mu}_B)$ in calculations of χ_{11}^{BS}/χ_2^S, along with the agreement between determinations of the experimentally determined μ_S/μ_B with QCD results, thus suggests that the experimental results for μ_S/μ_B are indeed sensitive to strange particle content at the time of freeze-out.

We start our discussion of cumulant ratios at finite temperature and nonzero values of the chemical potentials by revisiting the analysis of the ratio of mean, $\chi_1^B(T,\hat{\mu}_B)$, and variance, $\chi_2^B(T,\hat{\mu}_B)$, of net baryon-number density distributions

$$R_{12}^B = \frac{\chi_1^B(T,\hat{\mu}_B)}{\chi_2^B(T,\hat{\mu}_B)}$$

$$= \hat{\mu}_B \left(1 + s_1 \frac{\chi_{11}^{BS}}{\chi_2^B} + q_1 \frac{\chi_{11}^{QS}}{\chi_2^B}\right) + \mathcal{O}(\hat{\mu}_B^3), \quad (18)$$

where we again choose $n_S = 0$, and $n_Q/n_B = 0.4$.

The ratio $R_{12}^B(T,\hat{\mu}_B)$ has been analyzed by us previously and was shown in [17] in a $\hat{\mu}_B$-range relevant for the analysis of higher order cumulants. In Fig. 5 we show $R_{12}^B(T,\hat{\mu}_B)$ in a larger range of $\hat{\mu}_B$ values. The continuum
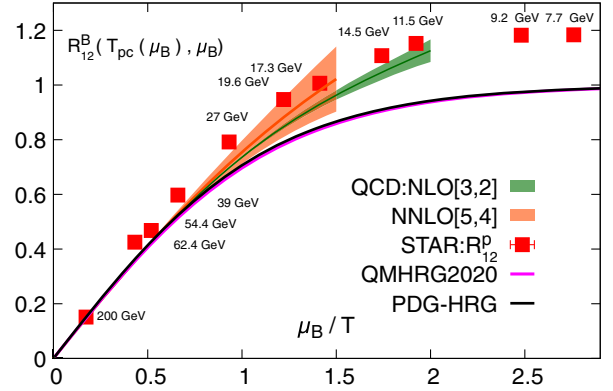

FIG. 5.   The ratio $R_{12}^B(T(\mu_B),\mu_B)$ on the pseudocritical line in $(2+1)$-flavor QCD versus $\hat{\mu}_B$ obtained for strangeness neutral matter with $n_Q/n_B = 0.4$. The bands show continuum estimates for next-to-leading (NLO [3, 2]) and next-to-next-to-leading (NNLO [5, 4]) order Taylor expansion results on the pseudocritical line that have been obtained from fits to data obtained in simulations on lattices with temporal extent $N_\tau = 8$ and 12 (see also discussion in the text). Also shown are results obtained by the STAR Collaboration for the corresponding proton cumulant ratio, R_{12}^p for various beam energies $\sqrt{s_{NN}}$ [33]. Results from [13] have been used to convert $\sqrt{s_{NN}}$ to thermal parameters $(T_f, \hat{\mu}_B^f)$. Furthermore, we show recent results for R_{12}^p obtained by the STAR Collaboration [34]. For data taken at two new beam energies, $\sqrt{s_{NN}} = 9.2$ and 17.3 GeV we used the parametrization of interpolating curves for freeze-out parameters given in [12]. Solid curves show results from HRG model calculations using the PDG-HRG and QMHRG2020 particle lists, respectively.

estimates based on up to $\mathcal{O}(\hat{\mu}_B^5)$ Taylor series for the net baryon-number density, χ_1^B, and a $\mathcal{O}(\hat{\mu}_B^4)$ Taylor series for the net baryon number fluctuations, χ_2^B (NNLO [5, 4]) shown in this figure are statistically well controlled for $\hat{\mu}_B \leq 1.5$. For large values of the chemical potential, $\hat{\mu}_B \leq 2$, we only show the result (NLO [3, 2]) based on $\mathcal{O}(\hat{\mu}_B^3)$ and $\mathcal{O}(\hat{\mu}_B^2)$ Taylor series for χ_1^B and χ_2^B, respectively. These continuum estimates are obtained from fits to data taken on lattices with temporal extent $N_\tau = 8$ and 12. As can be seen, the ratio R_{12}^B starts to deviate from HRG model calculations at about $\hat{\mu}_B \simeq 1$. The Taylor series, however, is still well controlled at least up to $\hat{\mu}_B \simeq 1.5$. We compare $R_{12}^B(T,\hat{\mu}_B)$, calculated in $(2+1)$-flavor QCD, with the corresponding ratio of net proton-number and its variance, $R_{12}^p(\sqrt{s_{NN}})$, [33] as follows. In order to convert the experimental control parameter, $\sqrt{s_{NN}}$, to a chemical potential value on the freeze-out line we use the set of freeze-out temperatures (T_f) and baryon chemical potentials (μ_B^f) determined from the analysis of particle yields using fits based on the thermodynamics of a hadron gas in the grand canonical ensemble [13,33].

As can be seen in the figure, the experimental results for $R_{12}^p(T_f,\mu_B^f)$ are close to the line of values for $R_{12}^B(T,\mu_B)$ on the pseudocritical line. We thus determined a set of

TABLE I. The left hand column lists the various RHIC beam energies, $\sqrt{s_{NN}}$, used by the STAR collaboration [33,34] for their measurements of net proton-number cumulants and $B - S$ correlations. The three columns in the middle give the chemical potentials and the temperature values on the pseudocritical line that correspond to $R_{12}^B = R_{12}^p$. The last three columns show corresponding freeze-out parameters obtained by fitting particle yields to a hadronization model based on the grand canonical ensemble [13]. Results for $\sqrt{s_{NN}} = 14.5$ and 54.4 GeV are taken from [33]. For $\sqrt{s_{NN}} = 9.2$ and 17.3 GeV we used the parametrization of interpolating curves for freeze-out parameters given in [12].

RHIC beam energy	QCD, pseudocritical line: using R_{12}^p			HIC, freeze-out line: using yields		
$\sqrt{s_{NN}}$ [GeV]	μ_B [MeV]	μ_S [MeV]	T_{pc} [MeV]	μ_B [MeV]	μ_S [MeV]	T_{ch} [MeV]
7.7	$\cdots$	$\cdots$	$\cdots$	398.2(16.4)	89.5(6.0)	144.3(4.8)
9.2	$\cdots$	$\cdots$	$\cdots$	358.3	$\cdots$	144.4
11.5	297.9(12.4)	73.5(4.8)	148.9(2.9)	287.3(12.5)	64.5(4.7)	149.4(5.2)
14.5	274.8(9.1)	68.2(3.7)	150.1(2.6)	264	$\cdots$	151.6
17.3	245.3(6.5)	61.3(2.8)	151.6(2.2)	218.6	$\cdots$	154.7
19.6	222.3(4.7)	55.7(2.2)	152.5(2.0)	187.9(8.6)	43.2(3.8)	153.9(5.2)
27.0	170.5(2.1)	42.9(1.3)	154.2(1.6)	144.4(7.2)	33.5(3.6)	155.0(5.1)
39.0	120.2(1.3)	30.3(1.2)	155.4(1.5)	103.2(7.4)	24.5(3.8)	156.4(5.7)
54.4	89.3(0.9)	22.5(0.6)	155.9(1.5)	83	$\cdots$	160.0
62.4	81.5(0.8)	20.5(0.5)	156.0(1.5)	69.2(5.6)	16.7(3.3)	160.3(4.9)
200	28.3(0.3)	7.1(0.2)	156.4(1.5)	28.4(5.8)	5.6(3.9)	164.3(5.3)

freeze-out parameters obtained by demanding $R_{12}^p(\sqrt{s_{NN}}) = R_{12}^B(T_{pc}(\mu_B^f), \mu_B^f)$. In Table I we compare the thus determined set of freeze-out parameters, $\{\mu_B^f, T_{pc}(\mu_B^f)\}$, with the experimental set of freeze-out parameters, $\{\mu_B^f, T_{ch}\}$, obtained by comparing measured particle yields to hadronization models [12–14].

As can be seen in Fig. 5, NLO and NNLO QCD results agree well with each other up to $\hat{\mu}_B \simeq 1.5$, where the errors of the NNLO expansion start getting large. In Table I, we tabulate the freeze-out parameters determined from R_{12}^p using NLO QCD results for $R_{12}^B(T, \hat{\mu}_B)$ and they agree well with the freeze-out parameters $\{T_f, \hat{\mu}_B^f\}$ obtained from particle yields down to $\sqrt{s_{NN}} \simeq 17.3$ GeV, which also corresponds to $\hat{\mu}_B \simeq 1.5$. For smaller $\sqrt{s_{NN}}$ or $\hat{\mu}_B \simeq 2.0$ the NNLO lattice QCD results have too large errors for a detailed quantitative comparison. Results from the NLO expansion are, however, still in good agreement with the STAR data down to $\sqrt{s_{NN}} \simeq 11.5$ GeV. In order to compare QCD results with STAR data at even lower beam energies statistically well controlled higher order Taylor series will be necessary.

It also should be noted that the experimentally determined R_{12}^p becomes larger than unity for $\sqrt{s_{NN}} \lesssim 17.3$ GeV. This is consistent with lattice QCD results for R_{12}^B, which become larger than unity for $\hat{\mu}_B \gtrsim 1.3$ or $\mu_B \gtrsim 200$ MeV. On the other hand, HRG model calculations based on noninteracting, pointlike hadrons will always lead to $R_{12}^B(T, \hat{\mu}_B) < 1$. The experimental data thus seem to reflect interactions in strong-interaction matter at freeze-out (on the pseudocritical line) that go beyond those taken care of in HRG models through the presence of a tower of excited states and resonances.

We give a comparison of the chemical potentials and pseudocritical temperatures on the pseudocritical line, $\{T_{pc}(\hat{\mu}_B), \mu_B\}$, that are obtained by demanding $R_{12}^B = R_{12}^p$ and the freeze-out parameters, $\{T_f, \mu_B^f\}$, obtained from HRG model fits to measured hadron yields in Table I.

B. Strangeness correlations on the pseudocritical line

In Fig. 6 (left) we show results for the ratio χ_{11}^{BS}/χ_2^S and compare with preliminary results for this ratio obtained by the STAR Collaboration [24]. As can be seen the Taylor series for the ratio χ_{11}^{BS}/χ_2^S converges well at least for $\hat{\mu}_B \lesssim 1.5$. Similar to the observation made for other observables results in $(2 + 1)$-flavor QCD and HRG model calculations based on the QMHRG2020 particle list also agree well in this $\hat{\mu}_B$-range. The preliminary STAR results, however, agree well with the QCD result only for $\sqrt{s_{NN}} = 62.4$ and 39 GeV. For smaller $\sqrt{s_{NN}}$ differences are significant. We note that this difference does not arise from a possible ambiguity in relating values of $\sqrt{s_{NN}}$ to values for $\hat{\mu}_B$ derived from experimental data.

As discussed above correlations between electric charge and strangeness are closely related to χ_{11}^{BS}. On the pseudocritical line and for conditions met in heavy ion collisions ($n_S = 0$, $n_Q/n_B = 0.4$) violations of the sum rule, Eq. (14), are smaller than 0.5% for $\hat{\mu}_B \leq 2$, which covers almost the entire range of the RHIC BES-II energy range in collider mode. In Fig. 6 (right) we show the ratio χ_{11}^{QS}/χ_2^S on the pseudocritical line and also compare with preliminary STAR results for χ_{11}^{BS}/χ_2^S [24] that have been converted to χ_{11}^{QS}/χ_2^S using Eq. (14).

Also shown in this figure is a result for χ_{11}^{QS}/χ_2^S obtained in [10] from particle yields measured by the
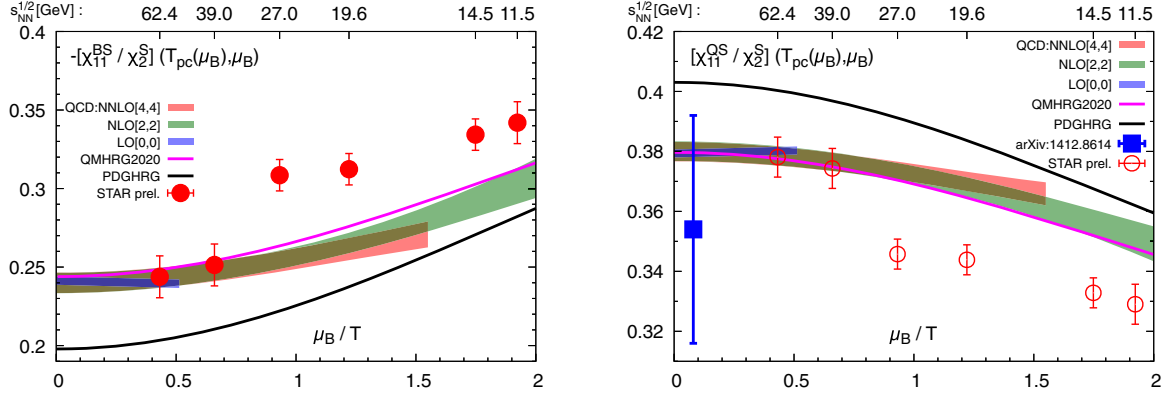
FIG. 6. Left: correlation between net strangeness and net baryon-number densities normalized to the second order cumulant of strangeness fluctuations on the pseudocritical line. The bands show continuum estimates for second and fourth order Taylor expansion results on the pseudocritical line that have been obtained from fits to data obtained in simulations on lattices with temporal extent $N_\tau = 8$ and 12. In the case of fourth order expansion we show results only up to $\mu_B/T = 1.5$. Right: same as left hand figure but for correlations between net strangeness and net electric charge densities. The data shown in the left hand figure use the preliminary results for χ_{11}^{BS}/χ_2^S obtained by the STAR Collaboration [24]. Data points shown in the right hand figure are obtained from the STAR data making use of the relation given in Eq. (10). Also shown in this figure is the result obtained in [10] from an analysis of ALICE data on strange particle yields (see also discussions in the text).

ALICE collaboration. This result has been obtained using data on strange particle yields, obtained by the ALICE Collaboration at the LHC [8,35]. The second order cumulants χ_2^S, χ_{11}^{BS} and χ_{11}^{QS} have been constructed from measured particle yields taking into account feed down corrections from ϕ-mesons and neutral kaons [10]. The second order cumulants, constructed in this way, obey the QCD sum rule, Eq. (14), except for contributions arising from the feed down corrections. As pointed out in [10] certain decay channels, contributing in particular to χ_{11}^{BS}, are not known experimentally. Moreover, it is difficult to take care of feed-down corrections arising from decays of experimentally not well controlled higher kaon resonances and additional strange hadrons. This suggests that an accurate experimental determination of χ_{11}^{BS} will remain to be difficult without achieving better control over contributions arising from additional resonances and their decay channels.

V. CONCLUSIONS

We pointed out that the determination of freeze-out parameters (T_f, μ_B^f, μ_S^f) from particle yields in heavy ion collisions is consistent with QCD parameters describing thermal conditions realized on the pseudocritical line for strangeness neutral matter with $n_Q/n_B = 0.4$. In particular, we find that at (T_f, μ_B^f, μ_S^f), corresponding to $\sqrt{s_{NN}} \geq 11.5$ GeV, the new results of the STAR collaboration obtained for the ratio of mean net proton number and the net proton number fluctuations, R_{12}^p, are in good agreement with R_{12}^B calculated in lattice QCD on the

pseudocritical line. Similarly we find that the ratio of strangeness and baryon chemical potentials, obtained from strange baryon yields and QCD calculations, respectively, are in good agreement. This suggests that the values of thermal control parameters (T, μ_B, μ_S), characterizing strong-interaction matter created at a given $\sqrt{s_{NN}}$, are well understood at least for $\sqrt{s_{NN}} \geq 11.5$ GeV.

Furthermore, we presented QCD results for the normalized baryon-number strangeness correlation χ_{11}^{BS}/χ_2^S as function of the baryon chemical potential $\hat{\mu}_B$ on the pseudocritical line $T_{pc}(\hat{\mu}_B)$. The results, based on fourth order Taylor series of second order cumulants, are shown to be well controlled for $\hat{\mu}_B \leq 1.5$ or equivalently $\mu_B \lesssim 200$ MeV. For conditions realized in heavy ion collisions at the time of freeze-out this corresponds to beam energies $\sqrt{s_{NN}} \geq 17.3$ GeV. Although results for χ_{11}^{BS}/χ_2^S obtained in QCD calculations agree well with experimental data for $\sqrt{s_{NN}} = 62.4$ GeV and 39 GeV, we observe significant differences for smaller beam energies. We thus conclude that there is some tension between current experimental results on strangeness and baryon number correlations and those appearing in strong-interaction matter on the pseudocritical line as described by equilibrium QCD thermodynamics. To verify or falsify that QCD thermodynamics can provide a good description of second order cumulant ratios of fluctuations and correlations of conserved charges, as measured in heavy ion collisions using various proxies, the origin of these differences clearly needs to be analyzed further.

All data presented in the figures of this paper can be found in [36].

APPENDIX: EXPANSIONS FOR SECOND ORDER CUMULANTS UP TO $\mathcal{O}(\hat{\mu}_B^4)$

In Eqs. (5)–(8) we gave the $\mathcal{O}(\hat{\mu}_B^2)$ expansions for the second order cumulants χ_{11}^{BS}, χ_{11}^{QS}, χ_2^S and χ_2^B. Here we give explicit expressions for expansions of these second order cumulants up to $\mathcal{O}(\hat{\mu}_B^4)$. This also requires expansions of the strangeness and electric charge chemical potentials up to $\mathcal{O}(\hat{\mu}_B^3)$ as defined in Eqs. (3) and (4). The coefficients s_i, q_i appearing in these expansions are given in [25].

With this we obtain for the second order cumulants the expansions,

$$
\chi_{11}^{BS}(T,\vec{\mu}) = \chi_{11}^{BS} + \frac{\hat{\mu}_B^2}{2!}[\chi_{31}^{BS} + 2s_1\chi_{22}^{BS} + s_1^2\chi_{13}^{BS} + 2q_1\chi_{211}^{BQS} + 2q_1s_1\chi_{112}^{BQS} + q_1^2\chi_{121}^{BQS}]
$$
$$
+ \frac{\hat{\mu}_B^4}{4!}[24\chi_{13}^{BS}s_1s_3 + \chi_{15}^{BS}s_1^4 + 24\chi_{112}^{BQS}q_1s_3 + 24\chi_{112}^{BQS}q_3s_1 + 4\chi_{114}^{BQS}q_1s_1^3 + 24\chi_{121}^{BQS}q_1q_3 + 6\chi_{123}^{BQS}q_1^2s_1^2
$$
$$
+ 4\chi_{132}^{BQS}q_1^3s_1 + \chi_{141}^{BQS}q_1^4 + 24\chi_{22}^{BS}s_3 + 4\chi_{24}^{BS}s_1^3 + 24\chi_{211}^{BQS}q_3 + 12\chi_{213}^{BQS}q_1s_1^2 + 12\chi_{222}^{BQS}q_1^2s_1
$$
$$
+ 4\chi_{231}^{BQS}q_1^3 + 6\chi_{33}^{BS}s_1^2 + 12\chi_{312}^{BQS}q_1s_1 + 6\chi_{321}^{BQS}q_1^2 + 4\chi_{42}^{BS}s_1 + 4\chi_{411}^{BQS}q_1 + \chi_{51}^{BS}] + \mathcal{O}(\hat{\mu}_B^6), \tag{A1}
$$

$$
\chi_{11}^{QS}(T,\vec{\mu}) = \chi_{11}^{QS} + \frac{\hat{\mu}_B^2}{2!}[\chi_{211}^{BQS} + 2s_1\chi_{112}^{BQS} + s_1^2\chi_{13}^{QS} + 2q_1\chi_{121}^{BQS} + 2q_1s_1\chi_{22}^{QS} + q_1^2\chi_{31}^{QS}]
$$
$$
+ \frac{\hat{\mu}_B^4}{4!}[24\chi_{013}^{BQS}s_1s_3 + \chi_{15}^{QS}s_1^4 + 24\chi_{022}^{BQS}q_1s_3 + 24\chi_{22}^{QS}q_3s_1 + 4\chi_{24}^{QS}q_1s_1^3 + 24\chi_{31}^{QS}q_1q_3 + 6\chi_{33}^{QS}q_1^2s_1^2
$$
$$
+ 4\chi_{42}^{QS}q_1^3s_1 + \chi_{51}^{QS}q_1^4 + 24\chi_{112}^{BQS}s_3 + 4\chi_{114}^{BQS}s_1^3 + 24\chi_{121}^{BQS}q_3 + 12\chi_{123}^{BQS}q_1s_1^2 + 12\chi_{132}^{BQS}q_1^2s_1
$$
$$
+ 4\chi_{141}^{BQS}q_1^3 + 6\chi_{213}^{BQS}s_1^2 + 12\chi_{222}^{BQS}q_1s_1 + 6\chi_{231}^{BQS}q_1^2 + 4\chi_{312}^{BQS}s_1 + 4\chi_{321}^{BQS}q_1 + \chi_{411}^{BQS}] + \mathcal{O}(\hat{\mu}_B^6), \tag{A2}
$$

$$
\chi_2^B(T,\vec{\mu}) = \chi_2^B + \frac{\hat{\mu}_B^2}{2!}[\chi_4^B + s_1^2\chi_{22}^{BS} + 2s_1\chi_{31}^{BS} + 2q_1\chi_{31}^{BQ} + 2q_1s_1\chi_{211}^{BQS} + q_1^2\chi_{22}^{BQ}]
$$
$$
+ \frac{\hat{\mu}_B^4}{4!}[24\chi_{22}^{BS}s_1s_3 + \chi_{24}^{BS}s_1^4 + 24\chi_{211}^{BQS}q_1s_3 + 24\chi_{211}^{BQS}q_3s_1 + 4\chi_{213}^{BQS}q_1s_1^3 + 24\chi_{22}^{BQ}q_1q_3 + 6\chi_{222}^{BQS}q_1^2s_1^2
$$
$$
+ 4\chi_{231}^{BQS}q_1^3s_1 + \chi_{24}^{BQ}q_1^4 + 24\chi_{31}^{BS}s_3 + 4\chi_{33}^{BS}s_1^3 + 24\chi_{31}^{BQ}q_3 + 12\chi_{312}^{BQS}q_1s_1^2 + 12\chi_{321}^{BQS}q_1^2s_1
$$
$$
+ 4\chi_{33}^{BQ}q_1^3 + 6\chi_{42}^{BS}s_1^2 + 12\chi_{411}^{BQS}q_1s_1 + 6\chi_{42}^{BQ}q_1^2 + 4\chi_{51}^{BS}s_1 + 4\chi_{51}^{BQ}q_1 + \chi_6^B] + \mathcal{O}(\hat{\mu}_B^6) \tag{A3}
$$

$$
\chi_2^S(T,\vec{\mu}) = \chi_2^S + \frac{\hat{\mu}_B^2}{2!}[\chi_{22}^{BS} + s_1^2\chi_4^S + 2s_1\chi_{13}^{BS} + 2q_1\chi_{112}^{BQS} + 2q_1s_1\chi_{13}^{QS} + q_1^2\chi_{22}^{QS}]
$$
$$
+ \frac{\hat{\mu}_B^4}{4!}[24\chi_4^S s_1s_3 + \chi_6^S s_1^4 + 24\chi_{13}^{QS}q_1s_3 + 24\chi_{13}^{QS}q_3s_1 + 4\chi_{15}^{QS}q_1s_1^3 + 24\chi_{22}^{QS}q_1q_3 + 6\chi_{24}^{QS}q_1^2s_1^2
$$
$$
+ 4\chi_{33}^{QS}q_1^3s_1 + \chi_{42}^{QS}q_1^4 + 24\chi_{13}^{BS}s_3 + 4\chi_{15}^{BS}s_1^3 + 24\chi_{112}^{BQS}q_3 + 12\chi_{114}^{BQS}q_1s_1^2 + 12\chi_{123}^{BQS}q_1^2s_1
$$
$$
+ 4\chi_{132}^{BQS}q_1^3 + 6\chi_{24}^{BS}s_1^2 + 12\chi_{213}^{BQS}q_1s_1 + 6\chi_{222}^{BQS}q_1^2 + 4\chi_{33}^{BS}s_1 + 4\chi_{312}^{BQS}q_1 + \chi_{42}^{BS}] + \mathcal{O}(\hat{\mu}_B^6) \tag{A4}
$$

[1] V. Koch, A. Majumder, and J. Randrup, Phys. Rev. Lett. **95,** 182301 (2005).

[2] R. V. Gavai and S. Gupta, Phys. Rev. D **64,** 074506 (2001).

[3] C. R. Allton, S. Ejiri, S. J. Hands, O. Kaczmarek, F. Karsch, E. Laermann, C. Schmidt, and L. Scorzato, Phys. Rev. D **66,** 074507 (2002).

[4] M. D'Elia and M.-P. Lombardo, Phys. Rev. D **67,** 014505 (2003).

[5] S. Borsanyi, Z. Fodor, S. D. Katz, S. Krieg, C. Ratti, and K. Szabo, J. High Energy Phys. 01 (2012) 138.

[6] J. Adam *et al.* (STAR Collaboration), Phys. Rev. Lett. **126,** 092301 (2021).

[7] S. V. Afanasiev *et al.* (NA49 Collaboration), Phys. Rev. C **66,** 054902 (2002).

[8] B. Abelev *et al.* (ALICE Collaboration), Phys. Rev. C **88,** 044910 (2013).

[9] J. Adam *et al.* (STAR Collaboration), Phys. Rev. C **102,** 034909 (2020).

[10] P. Braun-Munzinger, A. Kalweit, K. Redlich, and J. Stachel, Phys. Lett. B **747,** 292 (2015).

[11] R. Bellwied, S. Borsanyi, Z. Fodor, J. N. Guenther, J. Noronha-Hostler, P. Parotto, A. Pasztor, C. Ratti, and J. M. Stafford, Phys. Rev. D **101,** 034506 (2020).

[12] A. Andronic, P. Braun-Munzinger, K. Redlich, and J. Stachel, Nature (London) **561,** 321 (2018).

[13] L. Adamczyk *et al.* (STAR Collaboration), Phys. Rev. C **96,** 044904 (2017).

[14] S. Acharya *et al.* (ALICE Collaboration), Phys. Rev. Lett. **133,** 092301 (2024).

[15] A. Bazavov *et al.* (HotQCD Collaboration), Phys. Lett. B **795,** 15 (2019).

[16] S. Borsanyi, Z. Fodor, J. N. Guenther, R. Kara, S. D. Katz, P. Parotto, A. Pasztor, C. Ratti, and K. K. Szabo, Phys. Rev. Lett. **125,** 052001 (2020).

[17] A. Bazavov *et al.*, Phys. Rev. D **101,** 074502 (2020).

[18] A. Bazavov *et al.* (HotQCD Collaboration), Phys. Rev. D **96,** 074510 (2017).

[19] A. Bazavov *et al.*, Phys. Rev. Lett. **113,** 072001 (2014).

[20] D. Bollweg, J. Goswami, F. Karsch, S. Mukherjee, and C. Schmidt, Acta Phys. Pol. B Proc. Suppl. **14,** 373 (2021).

[21] R. L. Workman *et al.* (Particle Data Group), Prog. Theor. Exp. Phys. **2022,** 083C01 (2022).

[22] D. Bollweg, J. Goswami, O. Kaczmarek, F. Karsch, S. Mukherjee, P. Petreczky, C. Schmidt, and P. Scior (HotQCD Collaboration), Phys. Rev. D **105,** 074511 (2022).

[23] D. Bollweg, J. Goswami, O. Kaczmarek, F. Karsch, S. Mukherjee, P. Petreczky, C. Schmidt, and P. Scior (HotQCD Collaboration), Phys. Rev. D **104,** 074512 (2021).

[24] H. Feng (for the STAR Collaboration), *Baryon-Strangeness Correlations in Au+Au Collisions at RHIC-STAR, 15th Workshop on Critical Point and Onset of Deconfinement, Berkeley* (2024), https://conferences.lbl.gov/event/1376/contributions/8784/attachments/5143/4945/hwfeng_CPOD 2024.pdf.

[25] A. Bazavov *et al.*, Phys. Rev. D **95,** 054504 (2017).

[26] D. Bollweg, J. Goswami, O. Kaczmarek, F. Karsch, S. Mukherjee, P. Petreczky, C. Schmidt, and P. Scior, 10.4119/unibi/2957724 (2021).

[27] F. Karsch, Nucl. Phys. **A967,** 461 (2017).

[28] C. Bonati, M. D'Elia, M. Mariti, M. Mesiti, F. Negro, and F. Sanfilippo, Phys. Rev. D **92,** 054503 (2015).

[29] R. D. Pisarski and F. Wilczek, Phys. Rev. D **29,** 338 (1984).

[30] W. Brylinski, M. Gazdzicki, F. Giacosa, M. Gorenstein, R. Poberezhnyuk, S. Samanta, and H. Stroebele, arXiv:2312 .07176.

[31] H. Adhikary *et al.* (NA61/SHINE Collaboration), arXiv: 2312.06572.

[32] M. M. Aggarwal *et al.* (STAR Collaboration), Phys. Rev. C **83,** 024901 (2011); **107,** 049903(E) (2023).

[33] M. Abdallah *et al.* (STAR Collaboration), Phys. Rev. C **104,** 024902 (2021).

[34] A. Pandav (for the STAR Collaboration), *Precision Measurement of Net-proton Number Fluctuations in Au+Au Collisions at RHIC, Berkeley, 15th Workshop on Critical Point and Onset of Deconfinement, Berkeley* (2024), https://conferences.lbl.gov/event/1376/contributions/8772/attach ments/5163/4984/CPOD2024_PandavA_e9.pdf.

[35] B. B. Abelev *et al.* (ALICE Collaboration), Phys. Rev. C **91,** 024609 (2015).

[36] D. Bollweg, H.-T. Ding, J. Goswami, F. Karsch, Swagato Mukherjee, P. Petreczky, and C. Schmidt, Dataset for "Strangeness-Correlations on the pseudo-critical line in (2+1)-flavor QCD", Bielefeld University, 10.4119/unibi/2992312 (2024).